International Journal of MATERIALS RESEARCH

Zeitschrift für METALLKUNDE

Original Contributions

J. A. Kotzurek et al.: Structural anisotropy in equal-channel angular extruded nickel revealed by dilatometric study

Jaromir Anatol Kotzurek^a, Wolfgang Sprengel^a, Maciej Krystian^b, Sanja Simic^c, Peter Pölt^c, Anton Hohenwarter^d, Reinhard Pippan^e, Roland Würschum^a

- ^aInstitute of Materials Physics, Graz University of Technology, Graz, Austria
- ^b AIT Austrian Institute of Technology, Department of Health and Environment, Wiener Neustadt, Austria
- ^cInstitute of Electron Microscopy and Nanoanalytics, Graz University of Technology, Graz, Austria
- ^dDepartment of Materials Physics, University of Leoben, Leoben, Austria
- ^eErich Schmid Institute of Materials Science, Austrian Academy of Sciences, Leoben, Austria

Structural anisotropy in equal-channel angular extruded nickel revealed by dilatometric study of excess volume

Structural anisotropy and excess volume in ultra-fine grained high-purity nickel prepared by equal-channel angular pressing (ECAP) is studied by means of dilatometry and compared with the processing route of high-pressure torsion. Both routes exhibit qualitatively similar three-stage behavior in length change upon defect annealing with a characteristic dependence on the measuring direction related to the deformation axes. Taking into account shape anisotropy of the crystallites, the length change in various directions can be quantitatively analyzed yielding direct access to the concentration of deformation-induced lattice vacancies, the vacancy relaxation, and the grain boundary expansion. The routes A12 and $\rm B_{C}12$ of ECAP are compared.

Keywords: Dilatometry; Equal-channel angular pressing; High-pressure torsion; Vacancy; Recrystallization

1. Introduction

In the past few years, difference dilatometry has proven a powerful absolute technique in order to quantify the amount of excess volume in ultrafine grained metals prepared by severe plastic deformation (SPD) [1, 2]¹. In particular, the absolute concentration of deformation-induced lattice vacancies and the grain boundary (GB) expansion as well as issues of structural relaxation, defect kinetics and aggolomeration could be determined focusing on SPD-processed Ni [4–6] and Cu [7, 8]. Studies of these kinds of defects are of pivotal importance since the atomistic processes, which occur during SPD-induced structural refinement and which give rise to the particular mechanical behaviour, are intimately related to structural defects available in these materials in highly abundant concentrations [9, 10].

Based on systematic dilatometric studies of ultrafine grained metals prepared by high-pressure torsion (HPT) [4–6, 8, 11], the present work aims at studying free volumes in Ni in detail after an entirely different deformation process, namely equal-channel angular pressing (ECAP). Dilatometric results contributed to an earlier study on ECAP-processed Ni [12]. However, there commercial grade nickel of lower purity (99.6 wt.%) was used, and it is well known that impurities significantly influence the annealing behavior of the different defects. Furthermore, no orientation dependence was measured. Now again, nickel

¹ Valiev et al. for the first time used dilatometry for the study of SPD-processed metals [3].

is used, however, this time with high purity (99.99+ wt.%). It serves well as a model system, on the one hand, because lattice vacancies in Ni are stable at ambient temperature [13], and, on the other, because the temperature regime of annealing of lattice vacancies is well separated from the stage of crystallite growth.

ECAP-processing, besides HPT, is the primary route for the preparation of ultrafine grained metals in bulk dimensions [14–16]. A comparison of these methods with respect to free volumes is of interest in view of the characteristic differences concerning structural refinement and physical properties of materials obtained by ECAP or HPT. Comparing, for example, mechanical behaviour of the two routes, a higher hardness is reported for HPT compared to ECAP, but the hardness of ECAP-processed samples is more homogeneous due to a more homogeneous straining process [17].

A characteristic feature of both HPT and ECAP is structural anisotropy which is also of relevance for the mechanical properties [18]. The pronounced shape-anisotropy of the crystallites after HPT-deformation is reflected by a substantial variation of the dilatometric length change with measuring direction both in the temperature regime where vacancies anneal out [6] and in the regime where excess volume associated with GBs dissappears during grain growth [5]. This anisotropic annealing behavior even offers the potential for measuring the vacancy relaxation [6]. In ECAP-processing the degree of homogeneity or anisotropy of grain shapes can be controlled by appropriate sample rotations between successive passes [19].

2. Experimental procedure

For ECAP-processing in the present work two rods of high-purity nickel (99.99+ wt.%, Goodfellow Inc.) with diameters of 20 mm and lengths of 100 mm were used. Both rods were subjected to N=12 passes (N: number of passes) at a constant ram speed of 6 mm s⁻¹, one with route A and one with route B_C, denoted A12 and B_C12 in the following, respectively. In the route B_C the samples are rotated by 90° in the same direction between subsequent passes in contrast to the route A without rotation (for definition see, e. g. [16]). Both deformation routes were performed in a die containing two channels intersecting at an angle of $\Phi=120^\circ$ (so-called inner angle); the outer part of the intersecting channels is curved over an angle range $\Psi=27.8^\circ$ (so-called outer angle). According to the relation [20]

$$\varepsilon = \frac{N}{\sqrt{3}} \left[2 \cot \left(\frac{\Psi}{2} + \frac{\Phi}{2} \right) + \Psi[\text{rad}] \csc \left(\frac{\Psi}{2} + \frac{\Phi}{2} \right) \right] \tag{1}$$

the applied deformation corresponds to a uniform equivalent strain ε of 0.6 per pass and 7.5 in total. During ECAP-processing the rods exceeded ambient temperature by a few degrees only.

From each of the rods prism-shaped samples with square bases $(2.5 \times 2.5 \times 7 \text{ mm}^3)$ were cut out by means of a precision circular saw with an SiC saw blade. Samples from various positions (both close to the center and close to the edge) were cut in three different orientations of the ECAP-processed rods, i.e., in extrusion (E), transverse (T) and normal (N) directions as schematically shown in Fig. 1a. From each orientation a reference sample for dilatometry was prepared by pre-annealing at 800 K.

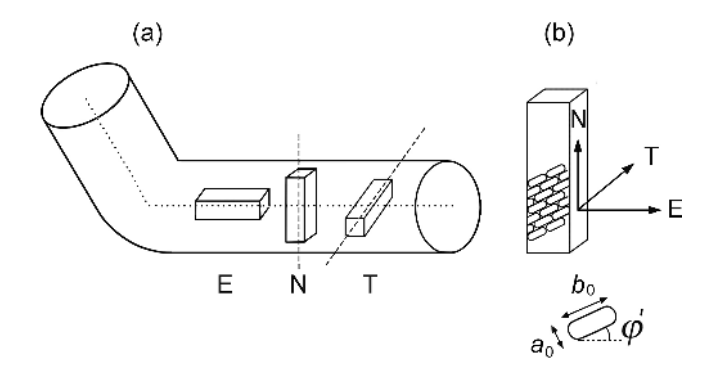


Fig. 1. a) Sketch of ECAP process and sample orientation. (E) denotes the extrusion direction parallel to the outlet channel, (N) the direction normal to the outlet channel within the plane of inlet and outlet channels, (T) the transverse direction perpendicular to the plane of inlet and outlet channels. (b) Dilatometry sample with inclination angle φ' of the elongated crystallites in the NE-plane with respect to the E-direction and the initial lengths a_0 and b_0 of the crystallite axes.

The dilatometric measurements were performed by means of a vertical high-precision difference dilatometer

(Linseis, model: L75VD500 LT) under a flow of 5 l h⁻¹ of high-purity argon (99.999%) (for details of the technique see, e.g., Sprengel et al. [1]). The length changes $\Delta L/L_0$ quoted in the following (Table 1, see below) denote net length changes determined as the difference to the pre-annealed reference sample prepared in the same orientation from the same rod. Therefore, variations of $\Delta L/L_0$ upon annealing are exclusively due to irreversible annealing processes in the ECAP-processed test sample. Heating was done from 273 K to 793 K with constant heating rates of 1.5, 2.5, 3.0, 5.0 and 6.0 K min⁻¹. Individual stages of defect annealing were identified from the derivative of the difference curve with respect to temperature which can directly be extracted from the time derivative of the measuring curve owing to the constant heating rate.

The dilatometric data for ECAP-processed Ni are compared with HPT-processed Ni measured under identical conditions. For this purpose, HPT deformation with 5 turns at room temperature up to an equivalent strain of 30 to 40 was performed on Ni of the same purity yielding a disk of 30 mm in diameter and 8 mm in height from which the dilatometer samples were cut. Details of the ongoing systematic studies [11] on HPT-processed Ni will be published elsewhere.

Microstructural characterization of the ultrafine-grained samples were performed by means of scanning electron microscopy (SEM) using a Zeiss Ultra 55 SEM with an electron backscatter detector. The micrographs were analyzed with the software ImageJ [21]. The crystallite sizes were determined by the line intercept method. In order to take into account shape anisotropy (see below), directions parallel and perpendicular to the axis of elongation with ca. 300 crystallites in each direction were evaluated by this technique.

3. Results

Figure 2 shows a representative SEM micrograph after ECAP-processing with the route A12, imaged in the NE plane, i.e., view in transverse direction (see Fig. 1). Clearly visible is an anisotropic crystallite shape. By means of com-

Table 1. Dilatometric length change $\Delta L/L_0$ measured for annealing stages A and B of Ni along the various measuring directions, i.e., in normal (N), transverse (T), and extrusion (E) directions of ECAP-samples (Fig. 1) or in axial (A) and tangential (T) directions of HPT samples [6]. Quoted in each case is the mean value obtained for the various 4–5 heating rates between 1.5 and 6 K min⁻¹ as well the mean value for the 2 similar heating rates of 2.5 and 3 K min⁻¹ (ECAP) or the mean value of samples for 3 K min⁻¹ (HPT: (A): 2, (T): 4). For $\Delta L/L_0|_A$ the variation between the start temperature of scanning and the onset of stage B is taken.

	Orientation	Number of samples	Stage A $\Delta L/L_0 _{\rm A}~(10^{-4})$	Stage B $\Delta L/L_0 _{\rm B}~(10^{-4})$
ECAP	N	4	-1.54 (±1.00)	-1.76 (±0.21)
(A12)		2	$-1.98 (\pm 0.31)$	-1.59 (±0.07)
	T	5	$-1.65 (\pm 0.19)$	-1.55 (±0.37)
		2	-1.65 (±0.32)	$-1.54 (\pm 0.05)$
	Е	4	+0.37 (±0.22)	-0.59 (±0.10)
		2	+0.29 (±0.13)	-0.59 (±0.02)
ECAP	N	5	-1.39 (±0.45)	-1.60 (±0.40)
$(B_C 12)$		2	$-1.52 (\pm 0.25)$	-1.71 (±0.49)
	T	5	-1.21 (±0.22)	-1.54 (±0.52)
		2	-1.38 (±0.11)	-1.47 (±0.37)
	Е	5	+0.30 (±0.39)	-0.88 (±0.20)
		2	+0.16 (±0.48)	-0.89 (±0.20)
HPT	A	4	-2.44 (±0.70)	-2.93 (±0.48)
		2	-2.48 (±0.77)	-2.19 (±1.77)
	Т	14	+0.91 (±0.30)	-1.30 (±0.31)
		4	+1.02 (±0.15)	-1.00 (±0.64)

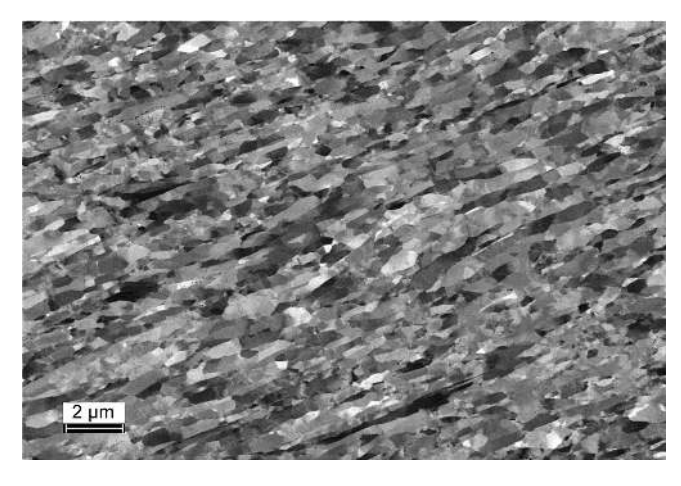


Fig. 2. Scanning electron micrograph of nickel after ECAP-processing via the A12 route. The sample is imaged in the NE plane, i. e., in transverse direction (see Fig. 1). The elongation axis of the crystallites is inclined by $\varphi'=23^\circ$ with respect to the extrusion direction.

parison with micrographs taken in the NT and TE plane (not shown) it can be concluded that the crystallite shape is elongated rather than platelet-shaped. Analyses of the micrographs in the NE plane by the line intercept method yield values $a_0 = (270 \pm 16)$ nm and $b_0 = (423 \pm 49)$ nm for the short and long axis, respectively. The elongation axis of the crystallites is inclined by $\varphi' = 23^{\circ}$ with respect to the extrusion direction (see sketch, Fig. 1b). For the route B_C12 the respective values are $a_0 = (298 \pm 41)$ nm, $b_0 = (372 \pm 61)$ nm, and $\varphi' = 33^{\circ}$ (see Table 2), i.e., the aspect ratio for the route A12 is higher than that for B_C12. The different degree of shape anisotropy can be attributed to the different strain paths of both methods; actually, the rotation

of the rod by 90° performed in the route B_C12 reduces to some extent the elongation [22]. Compared to ECAP-deformation, HPT-deformation results in a smaller crystallite size and a higher aspect ratio (see Table 2).

The obtained microstructure is in line with reports in literature, therefore, the dilatometric studies presented below can be safely considered as characteristic for ECAP-processed samples. Elongated grain shapes after ECAP-deformation of Ni are well documented in literature, not only after B_C12-processing [23], as applied here, but also after B_C4- [24] and B_C8-processing [25, 26]. It is also well documented that the degree of grain refinement for ECAP-deformation is not as high as for HPT-deformation [22]. As a reason therefore may be considered the reduced equivalent strain, i.e., 7.5 for the present ECAP-deformation, which is below the saturation regime achieved with the HPT-deformation applied here [27].

Turning to the results of the dilatometric measurements, Fig. 3 shows a comparison of the length changes $\Delta L/L_0$ for ECAP-processed Ni (route B_C12) in the transverse direction and for HPT-processed Ni in the axial direction measured during time-linear heating with the same rate of 3 K min⁻¹. Both deformation routes are characterized by the qualitatively same three-stage annealing behavior, albeit that of the ECAP-sample shifted towards higher temperatures. The first annealing stage, denoted stage A in the following, sets in at ca. 380 K (ECAP) or ca. 360 K (HPT), followed by a second sharp annealing stage (stage B) extending from ca. 500 K to ca. 580 K (ECAP) or from ca. 440 K to 500 K (HPT), as well as a third broad stage (C) up to maximum heating temperature of 793 K. The total length change $\Delta L/L_0$ is similar for ECAP and HPT.

The behavior of the series of HPT-samples, measured here for means of comparison, fully reproduces our earlier Table 2. Analyses of the dilatometric length changes $\Delta L/L_0$ of stages A and B. Stage A: Values for the vacancy concentration $C_{\rm V}$ and the vacancy relaxation r (Eq. (6)) deduced by means of Eq. (8) from the relative changes in stage (A) in normal (N, ECAP) (HPT: tangential, T) and extrusion (E) (HPT: axial, A) directions. Stage B: Grain boundary expansion $e_{\rm GB}$ calculated according to Eq. (3) from the relative length change in stage (B) in normal (ECAP) (HPT: tangential) and extrusion (HPT: axial) directions. a_0 and b_0 denote the initial lengths of the axes of the elongated crystallites; φ denotes the angle between the axis of grain elongation and the plane perpendicular to the dilatometric measuring direction (see Fig. 1). For the analysis the mean values of the length changes measured for 2.5 and 3 K min⁻¹ (ECAP) or 3 K min⁻¹ (HPT) are used (see Table 1).

	EC	HPT				
	A12	B _C 12				
a ₀ (nm)	270 ± 16 423 ± 49	298 ± 41 372 ± 61	120 ± 18 217 ± 15			
$b_0 (\text{nm})$	423 ± 49	372 ± 01	217 ± 13			
Stage A						
$\Delta L/L_0 _{\rm A}~(10^{-4})$	-1.98 (N)		-2.44 (A)			
φ	23° (N)		0 (A)			
$\Delta L/L_0 _{\rm A}~(10^{-4})$	+0.29 (E)		+0.90 (T)			
φ	67° (E)		90° (T)			
$C_{\rm V} (10^{-4})$	8.6		6.8 ^a			
r	0.50		0.40 ^a			
Stage B						
$\Delta L/L_0 _{\rm B}~(10^{-4})$	-1.76 (N)	-1.60 (N)	-2.19 (A)			
φ	23° (N)	33° (N)	0 (A)			
$e_{\rm GB}~(10^{-10}~{\rm m})$	0.50 (N)	0.51 (N)	0.26 (A)			
$\Delta L/L_0 _{\rm B}~(10^{-4})$	-0.59 (E)	-0.82 (E)	-1.30 (T)			
φ	67° (E)	57° (E)	90° (T)			
$e_{\rm GB}~(10^{-10}~{\rm m})$	0.23 (E)	0.31 (E)	0.28 (T)			

^a Kotzurek et al. [6]

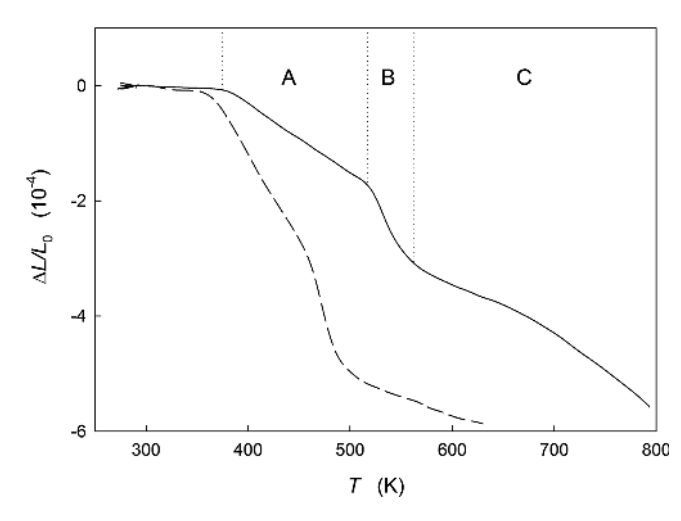
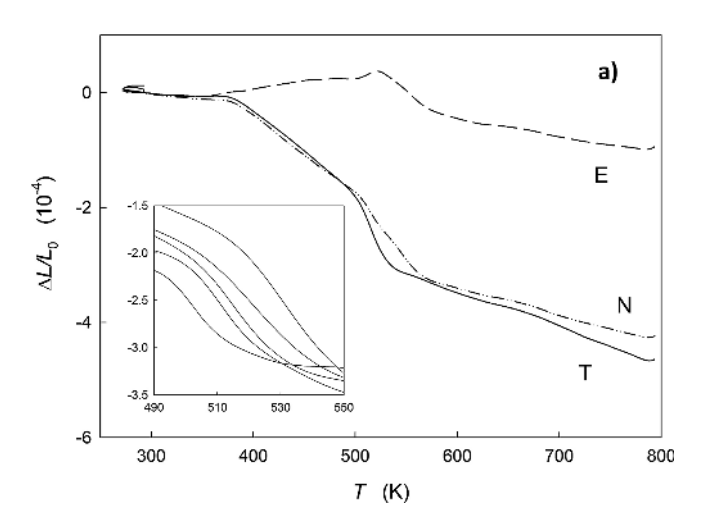


Fig. 3. Temperature dependence of relative length change $\Delta L/L_0$ of ultrafine-grained Ni samples upon time-linear heating with a rate of 3 K min⁻¹ after ECAP-processing, route B_C 12 (solid line, transverse direction) or HPT-processing (dashed line, axial direction). (A), (B), (C) denote the various regimes of annealing, the temperature regimes of which are marked for ECAP-processed Ni. In (A) or (B) annealing of predominantly lattice vacancies or grain growth occurs, respectively.

study on HPT-processed Ni [4, 5]. According to this study, stage B coincides with the strong crystallite growth and reflects the annealing out of free volume associated with grain boundaries (GB). Stage A is the regime where lattice vacancies become mobile in crystalline Ni. This stage is considered to arise primarily from the annealing-out of deformation-induced lattice vacancies at GBs. In addition, relaxation of GBs may contribute to stage A [5]. As outlined in more detail for HPT-processed Cu, which exhibits a qualitatively similar three stage behavior, stage C is primarily discussed in the context with the shrinkage of deformation-induced nanovoids [8]. Annealing of remnant dislocations during the process of grain growth likely contributes only to a minor extent to the length contraction (see [5]).

The orientation-dependence of the length changes $\Delta L/L_0$ for ECAP-processed Ni is shown representatively in Fig. 4 (part a: route A12; b: route B_C12) for the heating rate of 3 K min⁻¹. For both the route A12 and the route B_C12 rather similar length changes in transverse and normal directions occur in stage A as well as in stage B. Moreover, the changes for two routes are similar. This also holds for the



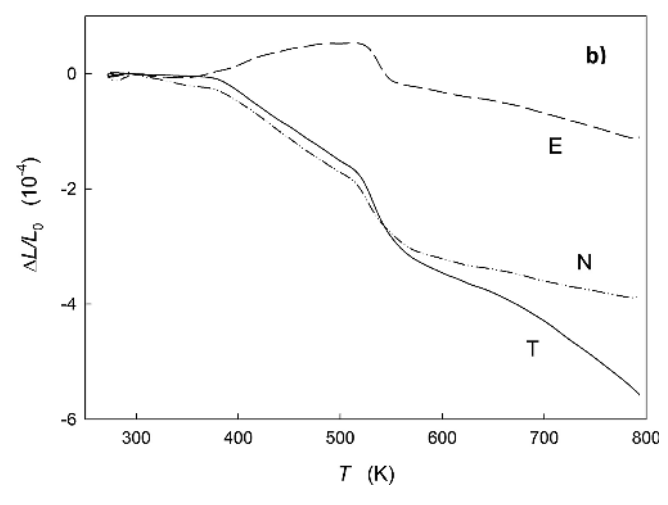


Fig. 4. Temperature dependence of relative length change $\Delta L/L_0$ of ECAP-processed Ni (a: route A12, b: route B_C12) measured upon time-linear heating rate of 3 K min⁻¹ in normal (N), transverse (T), and extrusion (E) directions. The inset in (a) shows the temperature shift of stage B with the heating rate (from left to right: 1.5, 2.5, 3.0, 5.0, 6.0 K min⁻¹) representatively for the transverse direction.

other heating rates, as a comparison of the mean value in each direction over all the heating rates shows (see summary of measuring data in Table 1). With increasing heating rate a shift of the stage B towards higher temperatures occurs (see inset in Fig. 4a).

Particularly remarkable is the length increase which is observed in the extrusion direction for stage A. For the samples prepared by the route A12 this finding is well reproducible, whereas for the route $B_{\rm C}12$ a significant scattering between various samples occurs as revealed by the large standard deviation of the mean $\Delta L/L_0$ -values in the E-direction (Table 1). It should be emphasized, however, that apart from the extrusion direction of the route $B_{\rm C}12$, the systematic measurements of more than 27 samples exhibit highly reproducible results (Table 1). Moreover, no systematic variation in the length change with the position, from the which the sample were cut from the ECAP-processed rod, can be discerned.

The extrusion direction differs from the normal and transverse directions not only with respect to stage A, but also with respect to stage B (Table 1). The length contraction $\Delta L/L_0|_{\rm B}$ in the E-direction is substantially reduced compared to that in the N- and T-directions, with the degree of reduction for A12 being more pronounced than for B_C12. Both findings reflect the structural anisotropy, as will be discussed next.

4. Analysis and discussion

For analysis and discussion of the results, at first stage B is considered. The temperature range of this sharp stage in the $\Delta L/L_0-T$ curves fits to the recrystallization stages found in microhardness and differential calorimetry measurements on ECAP-processed Ni [23, 25, 28]. For analyzing the length contraction due to release of excess grain boundary volume in stage B, we start with the relation

$$\left. \frac{\Delta L}{L_0} \right|_{\rm B} = e_{\rm GB} \left(\frac{1}{d_0} - \frac{1}{d_{\rm fin}} \right) \cong e_{\rm GB} \frac{1}{d_0} \tag{2}$$

according to Steyskal et al. [5]. $e_{\rm GB}$ denotes the expansion of the grain boundary which is the change of the volume with the grain boundary area, not to be confused with the GB thickness. A value for $e_{\rm GB}$ is deduced from the length contraction $\Delta L/L_0|_{\rm B}$ which occurs upon the elimination of GBs in the wake of crystallite growth from the initial diameter d_0 to the final diameter $d_{\rm fin}$ in the measuring direction. The approximation on the right-hand side of Eq. (2) holds because after the stage of crystallite growth $d_{\rm fin}$ is much larger than d_0 .

Since d_0 represents the initial distance between the GBs in the measuring direction, Eq. (2) can easily be adapted to the present situation where the axis of crystallite elongation is inclined with respect the measuring direction. We define φ as the angle between the axis of grain elongation and the plane perpendicular to the dilatometric measuring direction, which for measuring in the normal direction (N) corresponds to φ' as shown in the sketch in Fig. 1b. Due to the inclination, both the contribution of $e_{\rm GB}$ and the GB distance in the measuring direction are modified. Moreover, both the GBs along the short (a_0)

and the long initial axis (b_0) contribute to the length change which yields in summary:

$$\frac{\Delta L}{L_0} \Big|_{\rm B} = e_{\rm GB} \cos \varphi \frac{1}{\frac{a_0}{\cos \varphi}} e_{\rm GB} \sin \varphi \frac{1}{\frac{b_0}{\sin \varphi}}$$

$$= e_{\rm GB} \left(\frac{\cos^2 \varphi}{a_0} + \frac{\sin^2 \varphi}{b_0} \right) \tag{3}$$

The results of the analysis of stage B according to Eq. (3) are summarized in Table 2 for the measuring directions N and E for which the inclination angle has been determined by means of SEM. For comparison the results for HPT-processed Ni in the axial (A) direction and tangential (T) of the HPT-disk are also shown. For HPT-Ni nearly identical values of the GB expansion e_{GB} are obtained for both measuring directions. This shows that the dilatometric length change scales with number of GBs in measuring directions and supports the interpretation of this stage in terms of GB free volume. The mean value $\overline{e}_{GB} = 0.27 \times 10^{-10}$ m in both directons is slightly smaller than found previously for HPT-Ni ($\overline{e}_{GB} = 0.33 \times 10^{-10}$ m [5]). For the extrusion direction of the ECAP-processed samples similar values e_{GB} are obtained as for HPT-processed Ni (Table 2). Remarkably, however, the two similar e_{GB} -values of 0.50 and 0.51×10^{-10} m obtained for the normal direction of A12 and B_C12, respectively, are significantly higher.

The fact that the $e_{\rm GB}$ -values for the same direction of A12 and B_C12 are similar, although the ratio $(\Delta L/L_0|_{\rm B(N^-dir.)})/(\Delta L/L_0|_{\rm B(E^-dir.)})$ of the two directions is higher for A12 than for B_C12, shows that this different ratio is caused by the different degree of shape anisotropy. The different $e_{\rm GB}$ -values in E- and N-directions show, on the other hand, that both in A12 and B_C12 the length change in stage B does not scale with the number of GBs in the respective direction, but exhibits a characteristic orientation dependence. Various reasons for the higher length contraction in the normal direction compared to the extrusion direction may be taken into consideration, such as

- 1. a variation of the GB excess volume with the tilt angle of GBs as predicted theoretically [29], which would imply a higher amount of high-angle GBs in the N-direction compared to the E-direction
- 2. a preferred annealing out of lattice defects, such as remnant vacancies or nanovoids, at GBs in the N-direction during stage B owing to the initial shape anisotropy of the crystallites,
- a texture where the amount of crystallites with dense packing in N- or E-directions increases or decreases during recrystallization, respectively, or
- 4. an anisotropy of internal strains which anneal out in stage B.

An argument in favor of the second item would be the larger crystallite size compared to HPT-samples, so that after ECAP-processing lattice vacancies do not anneal out completely in stage A but partly in stage B only. Point defect annealing in stage B may either occur due to diffusion of the defect to GB sinks (similar to stage A, see below) or, else, due to the GB migration. A quantitative assessment of the other mentioned issues demands further structural investigations, such as mapping of the misorientation of crystallites, texture analysis, and strain analysis.

In addition to the amplitude of stage B, the shift of this stage with increasing heating rate Φ towards higher temperatures can be quantitively analyzed (see inset of Fig. 4). For this purpose the position of the stage as defined by the temperature $T_{\rm max}$ of the maximum transformation rate is derived from the peak position of the derivative $d(\Delta L/L_0)/dT$ of the length change curve (not shown). According to Kissinger [30]

$$\frac{\Phi}{T_{\text{max}}^2} = A \exp\left(-\frac{Q}{k_{\text{B}}T_{\text{max}}}\right) \tag{4}$$

the variation of $T_{\rm max}$ with Φ yields the energy Q of the thermally activated underlying process $k_{\rm B}$: Boltzmann constant). The Kissinger plot is shown in Fig. 5. For the ECAP-processed samples the data for the extrusion direction are omitted due to large scattering.

Apart from the shift of stage B towards higher temperatures in the ECAP-processed samples compared to the HPT-processed ones, which became visible in the $\Delta L/L_0-T$ dilatometer curve (Fig. 3), the Kissinger plot in addition clearly reveals a shift of the stage B for the route B_C12 towards higher temperatures compared to A12 (Fig. 5). For HPT-processed Ni the identical activation energy $Q=1.20~{\rm eV}$ is derived as found in our earlier measurements on similarly processed samples [4]. For the route B_C12 of ECAP-processed samples, which exhibits the most pronounced temperature shift with respect to HPT-Ni, also a substantially higher activation energy of 1.42 eV is obtained.

The observed shift of the stage B correlates with the inital crystallite size which increases from HPT to ECAP, A12 and to ECAP, B_C12 (Table 2). Such a correlation between the inital crystallite size and the recrystallization temperature is a general trend; among others, variations of the driving force, stored energy, and nucleation rate with the crystallite size are considered as reasons [31].

Next, we analyse the length variation $\Delta L/L_0|_{\rm A}$ in stage A. As a striking feature, one should point out the irreversi-

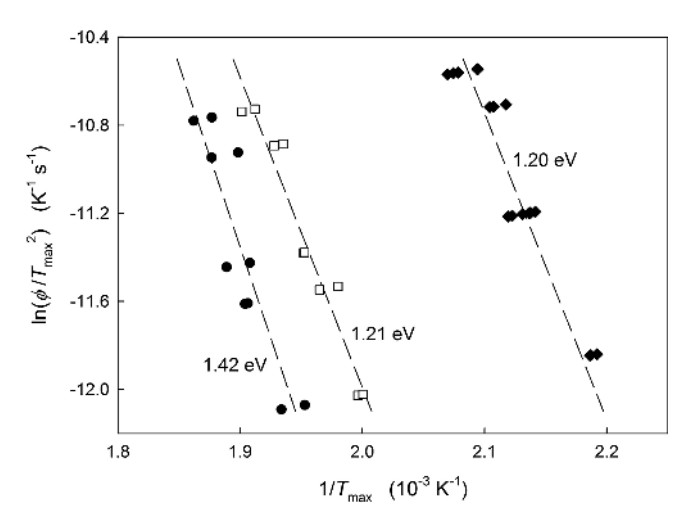


Fig. 5. Kissinger analysis of the temperatures $T_{\rm max}$ of the maximum length change rate applying the heating rate Φ . Plotted from left to right are the data for ECAP-processed Ni (route B_C12, A12) measured in directions T and N as well as the data for HPT-processed Ni. The activation energies Q from a linear fit (dashed lines) according to Eq. (4) are quoted.

ble length increase which is observed in the extrusion direction (E) during linear heating below the onset of stage B (Fig. 4). As discussed recently for HPT-processed Ni, such a characteristic variation with the measuring direction can be attributed to the anisotropic annealing out of relaxed lattice vacancies due to the elongated shape of the crystallites [6]. The simple notion is adopted that vacancies exclusively anneal out at grain boundaries which are enclosing the crystallites along their elongation axis owing to the reduced diffusion length required for reaching the GB sink. If the elongation axis is parallel (||) to the measuring direction, vacancies therefore anneal perpendicular to the measuring direction, causing a length increase

$$\left. \frac{\Delta L}{L_0} \right|_{\parallel} = +\frac{1}{3} C_{\text{V}} r \tag{5}$$

in the measuring direction since upon annealing relaxed vacancies are replaced by atoms [6]. The relaxation factor

$$r = \frac{\Omega - V_{\rm V}}{\Omega} = 1 - \frac{V_{\rm V}}{\Omega} \tag{6}$$

characterizes the relaxation of the vacancy volume $V_{\rm V}$ with Ω denoting the atomic volume. Annealing out of vacancies in measuring direction, i.e., with the elongation axis of the crystallites perpendicular (\bot) to the measuring direction, yields [6]:

$$\frac{\Delta L}{L_0} \bigg|_{1} = +\frac{1}{3}C_{V}r - \frac{1}{2}C_{V}$$
 (7)

Again as for stage B, we have to adapt the model to the present situation where the axis of crystallite elongation is inclined by an angle φ with respect to the plane perpendicular to the measuring direction. This yields the dilatometric length change in stage A due to the anisotropic annealing of lattices vacancies:

$$\frac{\Delta L}{L_0}\Big|_{A} = \cos\varphi\left(\frac{1}{3}C_{V}r - \frac{1}{2}C_{V}\right) + \sin\varphi\frac{1}{3}C_{V}r$$

$$= \frac{1}{3}C_{V}r(\cos\varphi + \sin\varphi) - \frac{1}{2}C_{V}\cos\varphi$$
(8)

Measuring the length changes $\Delta L/L_0|_{\rm A}$ in two directions yields a set of two equations of type (8), from which $C_{\rm V}$ and r can be calculated.

For HPT-processed Ni a vacancy concentration $C_{\rm V} = 6.8 \times 10^{-4}$ and a relaxation factor r = 0.40 is derived from the ratio of length changes $\Delta L/L_0|_{\rm A}$ in the axial and tangential directions as communicated recently (Table 2) [6]. For ECAP-processed Ni with the A12-route, the decrease of the length $\Delta L/L_0|_{\rm A}$ in the normal direction and its increase in the extrusion direction yields values for $C_{\rm V}$ of 8.6×10^{-4} and for r of 0.50 (Table 2). For the B_C12-route an analysis according to Eq. (8) appears inappropriate due to the enhanced scattering of the data, as mentioned above.

The roughly similar vacancy relaxation factor deduced for ECAP-processed Ni (route A12) compared to HPT-processed Ni supports the notion that stage A of the ECAP- sample is also predominantly due to vacancy annealing as it is considered for HPT [6]. This interpretation is also in line with the slight shift of stage A towards higher temperatures in ECAP-compared to HPT-Ni, because this shift reflects the increasing diffusion length of the vacancies for reaching the GB sinks. Both in ECAP- and HPT-processed Ni excess concentrations of deformation-induced lattice vacancies in the range of several 10⁻⁴ occur which, therefore, may be considered as characteristic for Ni prepared after severe plastic deformation.

The fact that the $\Delta L/L_0|_{\rm A}$ -variation in extrusion directions for the B_C12-route behaves not as systematically as for the A12-route, can simply be understood by the lower degree of shape anisotropy in the B_C12-samples. Obviously, the simple notion underlying the above presented model, according to which vacancies anneal exlusively perpendicular to the axial of elongation, does not hold for B_C12 due to the reduced shape anisotropy. Nevertheless, the variation of $\Delta L/L_0|_{\rm A}$ with measuring direction shows that a certain anisotropy of vacancy annealing also persists for B_C12.

Finally, we note the substantial influence of impurities on the thermal stability of free-volume related defects by comparing the present results on 99.99+ wt.% pure Ni with recent dilatometry measurements on ECAP-processed 99.6 wt.% pure Ni (route B_C4) [12]. The less pure Ni-samples exhibit a length contraction extending over the entire measuring range (Fig. 3 in Ref. [12]) without pronounced stages as observed here for high-purity Ni after ECAP- or HPT-processing. The amount of deformation-induced single vacancies is reduced in the less pure sample which is presumably related to vacancy–impurity complexes, evidence for which is derived from DSC [12]. In particular, crystallite growth is sluggish and shifted towards higher temperatures due to impurities [12].

So far only pure metals have been considered, however, as the preceding remarks suggest, it might be quite interesting to extend dilatometric studies to solid solutions or, in general, to binary alloys deformed by severe plastic deformation. For these materials it has been reported that during severe plastic deformation dynamic recrystallization can occur, giving rise, e.g., to dissolution of precipitates or decomposition of phases (see [32, 33]). Dilatometric techniques as presented here cannot directly be applied during the deformation process itself. But it might, however, be envisaged to study precipitation/dissolution processes in alloys during dynamic recrystallization by applying ex-situ studies to samples after different degrees of severe plastic deformation. It should be emphasized that in general dilatometry is a powerful tool for the analysis of dynamic processes. This has recently been demonstrated by the present authors in a high-resolution dilatometric in-situ study of formation, transformation and dissolution processes of hardening phases in a commercial aluminum alloy (AW6060) [34].

5. Conclusions

In summary, the major results of the present studies of structural anisotropy of ECAP-processed Ni by means of high precision dilatometry are as follows:

 Two annealing stages A and B of dilatometric length occur in ECAP-processed Ni similar to after HPT-deformation.

- The characteristic variation with the measuring directions (extrusion, transverse, normal) reveals a pronounced structural anisotropy.
- From stage A, a vacancy concentration in the range of several 10⁻⁴ and direct evidence of vacancy relaxation is derived.
- 4. From stage B, a GB expansion $e_{\rm GB}$ in the range of $(0.23-0.31)\times 10^{-10}$ m is deduced as typical for GBs.
- 5. The enhanced length change in stage B perpendicular to the extrusion direction does not exclusively arise from the shape anisotropy of the crystallites, but yields evidence for an additional source of anisotropy, such as texture, internal strains, or a variation of the GB type (low angle, high angle).

The present study clearly demonstrates the close correlation between structural anisotropy and dilatometric length change for the model system Ni, in which the temperature regimes of vacancy migration and crystallite growth are well separated. The extension of the studies to other systems, where these temperature regimes overlap, appears promising in the light of the present studies, because it could be shown that the effect of structural anisotropy can be readily taken into account for the analysis of dilatometric data. Moreover, in the field of structurally complex microstructures, such as ECAP-processed materials, novel application potentials for the direct and specific method of high-precision dilatometry may open up with the recently achieved progress in high-stability non-contact dilatometry [35].

The authors are indebted to M. Luckabauer (Inst. of Mater. Phys., TU Graz) for fruitful discussion. This work is financially supported by the Austrian Science Fund (FWF): P25628-N20.

References

- [1] W. Sprengel, B. Oberdorfer, E.-M. Steyskal, R. Würschum: J. Mater. Sci. 47 (2012) 7921. DOI:10.1007/s10853-012-6460-9
- [2] R. Würschum, B. Oberdorfer, E.-M. Steyskal, W. Sprengel, W. Puff, P. Pikart, C. Hugenschmidt, R. Pippan: Physica B 407 (2012) 2670–2675. DOI:10.1016/j.physb.2012.01.090
- [3] K.Y. Mulyukov, S.B. Khaphizov, R.Z. Valiev: Phys. Status Solidi A 133 (1992) 447. DOI:10.1002/pssa.2211330228
- [4] B. Oberdorfer, E.-M. Steyskal, W. Sprengel, R. Pippan, M. Zehetbauer, W. Puff, R. Würschum: J. Alloys Comp. 509S (2011) S309. DOI:10.1016/j.jallcom.2010.12.130
- [5] E.-M. Steyskal, B. Oberdorfer, W. Sprengel, M. Zehetbauer, R. Pippan, R. Würschum: Phys. Rev. Lett. 108 (2012) 055504. DOI:10.1103/PhysRevLett.108.055504
- [6] J.A. Kotzurek, É.-M. Steyskal, B. Oberdorfer, A. Hohenwarter, R. Pippan, W. Sprengel, R. Würschum: Appl. Phys. Lett. 109 (2016) 021906. DOI:10.1063/1.4958895
- [7] B. Oberdorfer, E.-M. Steyskal, W. Sprengel, W. Puff, P. Pikart, C. Hugenschmidt, M. Zehetbauer, R. Pippan, R. Würschum: Phys. Rev. Lett. 105 (2010) 146101. DOI:10.1103/PhysRevLett.105.146101
- [8] B. Oberdorfer, D. Setman, E.-M. Steyskal, A. Hohenwarter, W. Sprengel, M. Zehetbauer, R. Pippan, R. Würschum: Acta Mater. 68 (2014) 189–195. DOI:10.1016/j.actamat.2013.12.036
- [9] E. Schafler, G. Steiner, E. Korznikova, M. Kerber, M. Zehetbauer: Mater. Sci. Eng. A 410–411 (2005) 169. DOI:10.1016/j.msea.2005.08.070
- [10] D. Setman, E. Schafler, E. Korznikova, M.J. Zehetbauer: Mater. Sci. Eng. A 493 (2008) 116. DOI:10.1016/j.msea.2007.06.093
- [11] J.A. Kotzurek: PhD thesis, ongoing, Graz University of Technology, Austria (2016).
- [12] G. Reglitz, B. Oberdorfer, N. Fleischmann, J.A. Kotzurek, S.V. Divinski, W. Sprengel, G. Wilde, R. Würschum: Acta Mater. 103 (2016) 396. DOI:10.1016/j.actamat.2015.10.004

- [13] W. Wycisk, M. Feller-Kniepmeier: J. Nucl. Mater. 69–70 (1978) 616. DOI:10.1016/0022-3115(78)90293-3
- [14] T.G. Langdon: Acta Mater. 61 (2013) 7035. DOI:10.1016/j.actamat.2013.08.018
- [15] R.Z. Valiev, Y. Estrin, Z. Horita, T.G. Langdon, M.J. Zehetbauer, Y.T. Zhu: Mater. Res. Lett. 4 (2016) 1–21. DOI:10.1080/21663831.2015.1060543
- [16] R.Z. Valiev, T.G. Langdon: Prog. Mater. Sci. 51 (2006) 881. DOI:10.1016/j.pmatsci.2006.02.003
- [17] N. Lugo, N. Llorca, J.M. Cabrera, Z. Horita: Mater. Sci. Eng. A 477 (2008) 366. DOI:10.1016/j.msea.2007.05.083
- [18] R. Pippan, A. Hohenwarter: Mater. Res. Lett. 4 (2016) 127. DOI:10.1080/21663831.2016.1166403
- [19] V. Stolyarov, Y. Zhu, I. Alexandrov, T. Lowe, R.Z. Valiev: Mater. Sci. Eng. A 299 (2001) 59. DOI:10.1016/S0921-5093(00)01411-8
- [20] Y. Iwahashi, J. Wang, Z. Horita, M. Nemoto, T.G. Langdon: Scr. Mater. 35 (1996) 143. DOI:10.1016/1359-6462(96)00107-8
- [21] M.D. Abramoff, P.J. Magalhaes, S.J. Ram: Biophotonics Int. 11 (2004) 36.
- [22] R.Z. Valiev, R.K. Islamgaliev, I.V. Alexandrov: Prog. Mater. Sci. 45 (2000) 103. DOI:10.1016/S0079-6425(99)00007-9
- [23] K.S. Raju, M.G. Krishna, K.A. Padmanabhan, V.S. Sarma, N.P. Gurao, G. Wilde: J. Mater. Sci. 46 (2011) 2662. DOI:10.1007/s10853-010-5122-z
- [24] S.V. Divinski, G. Reglitz, I.S. Golovin, M. Peterlechner, R. Lapovok, Y. Estrin, G. Wilde: Acta Mater. 82 (2015) 11. DOI:10.1016/j.actamat.2014.08.064
- [25] A.P. Zhilyaev, G.V. Nurislamova, M.D. Baro, R.Z. Valiev, T.G. Langdon: Metall. Mater. Trans. A 33 (2002) 1865. DOI:10.1007/s11661-002-0197-z
- [26] N. Krasilnikov, W. Lojkowski, Z. Pakiela, R. Valiev: Mater. Sci. Eng. A 397 (2005). 330. DOI:10.1016/j.msea.2005.03.001
- [27] R. Pippan, S. Scheriau, A. Taylor, M. Hafok, A. Hohenwarter, A. Bachmaier: Ann. Rev. Mater. Res. 40 (2010) 210. DOI:10.1146/annurev-matsci-070909-104445
- [28] K. Neishi, Z. Horita, T.G. Langdon: Mater. Sci. Eng. A 325 (2002) 54. DOI:10.1016/S0921-5093(01)01404-6
- [29] J.J. Bean, K.P. McKenna: Acta Mater. 110 (2016) 246. DOI:10.1016/j.actamat.2016.02.040
- [30] H.E. Kissinger: J. Res. Nat. Bur. Stand. 57 (1956) 217. DOI:10.6028/jres.057.026
- [31] M. Hatherly, F.J. Humphreys, G.S. Rohrer, A. Rollett, in: F.J. Humphreys, M. Hatherly (Eds), Recrystallization and Related Annealing Phenomena, 2nd Ed., Elsevier Science, Amsterdam (2004) 215. DOI:10.1016/B978-008044164-1/50011-6

- [32] B. Straumal, A. Korneva P. Zieba: Arch. Civil Mech. Eng. 14 (2014) 242. DOI:10.1016/j.acme.2013.07.002
- [33] B.B. Straumal, V. Pontikis, A.R. Klimametov, A.A. Mazilkin, S.V. Dobatkin, B. Baertzky: Acta Mater. 122 (2017) 60. DOI:10.1016/j.actamat.2016.09.024
- [34] M. Luckabauer, E. Hengge, G. Klinser, W. Sprengel, R. Würschum: Proc. TMS Annual Meeting on Magnesium Technology (2017): In-situ Methods for Unraveling Structure-Property Relationships in Light Metals, accepted for publication.
- [35] M. Luckabauer, W. Sprengel, R. Würschum: Rev. Sci. Instr. 87 (2016) 075116. DOI:10.1063/1.4959200

(Received September 7, 2016; accepted November 29, 2016; online since January 11, 2017)

Correspondence address

Dr. Roland Würschum Institute of Materials Physics Graz University of Technology Petersgasse 16 8010 Graz Austria

Tel.: +43 316 873 8480 Fax: +43 316 873 108480 E-Mail: wuerschum@tugraz.at

Web: https://www.tugraz.at/institute/imp/home/

Bibliography

DOI 10.3139/146.111463 Int. J. Mater. Res. (formerly Z. Metallkd.) 108 (2017) 2; page 81–88 © Carl Hanser Verlag GmbH & Co. KG ISSN 1862-5282